An Extensive Study of Structural, Dielectric, Magnetic and Optical Properties of Multiferroic $CoFe_2O_4$-$BaTiO_3$ and $CoFe_{1.7}Mn_{0.3}O_4$-$BaTiO_3$ Core-Shell Type Composites

Sourav Sarkar, J. Shah, R. K. Kotnala, M. C. Bhatnagar

Abstract*— Multiferroic $CoFe_2O_4$ -$BaTiO_3$ and $CoFe_{1.7}Mn_{0.3}O_4$ - $BaTiO_3$ core-shell type composites (CFO-BTO and CFMO-BTO) were synthesized by conventional wet chemical method which combined two processes: co–precipitation method and sol–gel technique. X-ray diffraction (XRD) analysis confirms presence of both phases and average crystallite sizes for them were calculated to be in the range 15 – 30 nm. HRTEM micrographs ensure proposed core-shell like structure and verify estimated particle size from XRD data. No impurity other than the constituent elements has been found in the EDX spectra of individual phases as well as composites. SEM images of the powder form suggest presence of two different phases in the composites while images of the pellet forms show particle formation of both phases with dense microstructure. Variation of dielectric parameters with temperature at different frequencies yielded expected results with some interesting response around magnetic Curie temperature (T_c) for CFMO-BTO composite. Magnetic hysteresis loops were plotted for all these samples by applying a dc magnetic field in the range -5000 Oe to +5000 Oe. They show expected ferromagnetic behavior. Photoluminescence (PL) data was acquired using a laser excitation source of 266 nm. Emission peaks corresponding to individual phases (CFO, CFMO and BTO) as well as the composites were recorded and studied for the first time in core–shell composites.

***Index Terms*—Composites, Dielectric properties, Optical properties, Sol-gel processes**

I. INTRODUCTION

Multiferroics have been drawing a lot of attention among the researchers throughout the world since past decade due to their wide potential range of application such as magnetoelectric memory devices, transducers, filters etc. [1, 2]. Multiferroics largely refer to a class of materials where different ferroic orders (e.g. ferroelectric, ferromagnetic, ferroelastic) are present simultaneously. Among them, magnetoelectric multiferroics are those where ferroelectric (or paraelectric or anti-ferroelectric) and ferromagnetic (or paramagnetic or anti-ferromagnetic) phases coexist. The beauty of these materials lies in the fact that they can be polarized by applying a magnetic field, and can be magnetized by applying an electric field which enables us to increase one degree of freedom. Since ferroelectricity and ferromagnetism are two mutually exclusive phenomena, single phase multiferroics with significant value of magnetoelectric coefficient (α_E) are rare in nature [1-4]. Composite multiferroics offer a solution to this shortcoming.

Coexistence of different ferroic orders is not enough for a good composite multiferroic material as it needs a strong coupling interaction between the phases. To achieve this, different research groups have synthesized different structures of composite materials [2]. Among them, core–shell structure offers a simple yet elegant way of having strong coupling interaction between the magnetostrictive and piezoelectric phase via strain–stress mechanism. Cobalt ferrite is a very well-known magnetic material with high magnetostriction coefficient (λ`) value. Any type of substitution in cobalt ferrite generally decreases the magnitude of λ`. But at the same time, the difference in resistivity between cobalt ferrite and barium titanate is so large that poling the composites becomes real difficult due to high leakage current. To bridge this difference to some extent, increment of resistivity of cobalt ferrite has been effectively done by some research groups through substitution of Mn and Zn at the site of Fe and Co respectively. Also substitution of Mn at the site of Fe has an effect in lowering the magnetic Curie temperature (T_C) of cobalt ferrite [5]. So we have tried an optimized substitution of Mn which has been done and verified by different research groups. This, at one hand, increases the resistivity and lowers T_C and on the other hand, does not decrease the value of λ` too much.

Here we have prepared CFO and CFMO by chemical co-precipitation method and finally used them as core material in BTO sol. The systems under study are (x) CFO – (1-x) BTO and (x) CFMO – (1-x) BTO where x= 0.3 and 0.4. Structural, dielectric, magnetic and optical characterizations have been performed on these samples and the results, along with their analysis have been presented here.

Revised Version Manuscript Received on July 10, 2016.

Sourav Sarkar, Physics Department, Indian Institute of Technology Delhi, New Delhi, India.

Dr. Jyoti Shah, Material Physics and Engineering, National Physical Laboratory, New Delhi, India.

Dr. R. K. Kotnala, Material Physics and Engineering, National Physical Laboratory, New Delhi, India.

Dr. Mukesh Chander Bhatnagar, Physics Department, Indian Institute of Technology Delhi, New Delhi, India.

II. EXPERIMENTAL DETAILS

$Co(NO_3)_2$, $Fe(NO_3)_3$and $Mn(NO_3)_2$ were the starting reagents in preparation of CFO and CFMO nanoparticles by co-precipitation method. They were taken in stoichiometric ratio and were mixed together in aqueous solution using minimum amount of de-ionized water. 10M NaOH solution was used as precipitating agent. Both solutions were first heated to 65°C and NaOH solution was slowly added to the other solution under constant stirring. Black precipitate formed immediately and the temperature of the solution was raised to 80°C for next half an hour for well growth of the desired spinel phase. Once the solution cooled down, the precipitate was filtered and washed with deionized water several times. Finally it was dried using an IR lamp and was grinded into fine powder before collection.

BTO sol was prepared in nitrogen environment using barium hydroxide and titanium n-butoxide, mixed in stoichiometric ratio in minimum amount of glacial acetic acid which was heated at 90°C. Stearic acid was used as chelating agent. A clear sol was produced in which already prepared and calculated amount of CFO nanoparticles were dispersed maintaining desired weight percentage with respect to BTO. This sol was vigorously sonicated for an hour to ensure uniform distribution of the nanoparticles throughout. Then it was dried at 80°C for eight hours for gel formation. Before drying, 2 methoxy – ethanol was added to the sol to enhance gel formation. Finally obtained gel was sintered at 900°C for four hours and was grinded into fine powder. CFMO-BTO composites were prepared in similar fashion. Structural, magnetic and optical characterizations were performed on the powder form. For dielectric characterization, we pelletized the samples in disc form with an average diameter of 9 mm and thickness 1-1.5 mm, applying a pressure of 6 tons/cm^2 in a hydraulic press. Pellets with 30% magnetostrictive phase were sintered at 1150°C for 12 hours and those with 40% magnetostrictive phase were sintered at 1135°C for 12 hours. While pellets of CFO and CFMO were sintered at 1050°C for 10 hours, sintering temperature and duration for pellet of BTO were 1200°C and 4 hours respectively. This kind of variation in sintering temperature was done keeping in mind that melting point of pure BTO is more than CFO or CFMO.

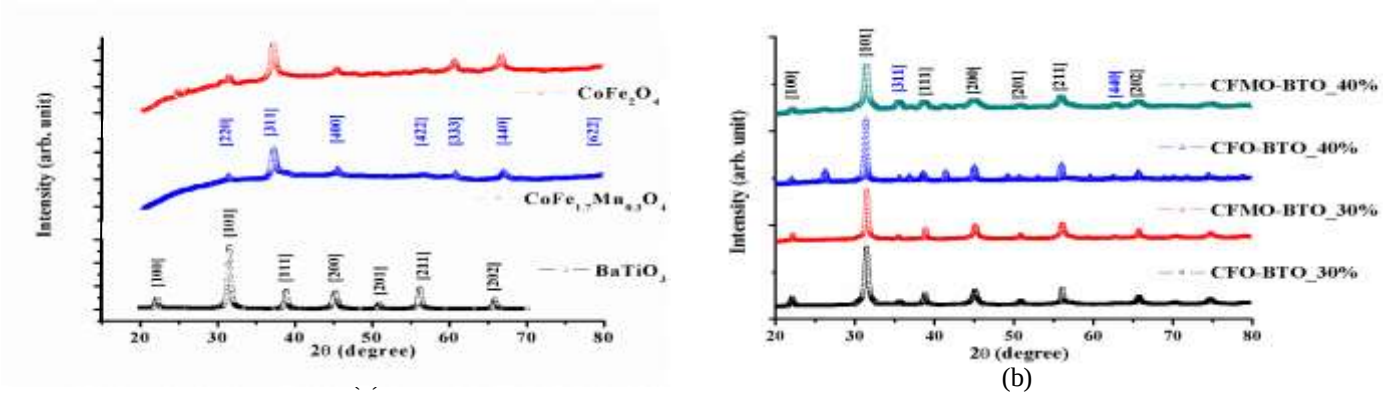

(b)

Fig. 1. (a) XRD patterns of CFO, CFMO and BTO and (b) XRD patterns of composite samples

We decreased sintering temperature as weight percentage of magnetostrictive phase in the composite increased [6] in such a way that it prevents melting and any kind of chemical reaction between the phases, but at the same time does not compromise with dense microstructure. These pellets were silver painted on both sides for electric connection. In this paper, we have named the samples with 30% of magnetostrictive phase; sample A (CFO – BTO_30%) and sample B (CFMO – BTO_30%) and samples with 40% of magnetostrictive phase are abbreviated as sample C (CFO – BTO_40%) and sample D (CFMO – BTO_40%).

Structural characterizations were done using a Phillips X'pert PRO Thin film X-ray diffractometer (CuK_α radiation; λ = 1.5406 Å), Technai G^2 20 transmission electron microscope (HRTEM), operated at 200 kV and a scanning electron microscope (SEM), model Carl Zeiss EVO 50. The dielectric properties were measured using HP4192A LF impedance analyzer. Hysteresis loops of the powder samples were recorded using Lakeshore 7304 Vibrating Sample Magnetometer (VSM) at room temperature. We recorded PL images at room temperature using a Perkin-Elmer PL spectrometer (model LS 55) with 266 nm laser excitation source.

III. RESULTS AND DISCUSSION

The x-ray diffraction patterns of individual phases and composites have been shown in Fig. 1.a and Fig. 1.b respectively. While all spinel peaks are present for both CFO and CFMO, perovskite peaks corresponding to BTO can clearly be seen in Fig. 1.a. No secondary peaks can be found ensuring presence of minimal or no impurity. In case of composites, all perovskite peaks are quite prominent while spinel peaks appear to be suppressed in Fig. 1.b. While one reason is the lesser amount of the magnetostrictive phase, it also suggests that the samples are core–shell in nature with BTO encapsulating the magnetostrictive phase [7]. We calculated the lattice parameters of individual phases for all the samples using Unit CELL software. The crystallite sizes corresponding to most prominent (311) peak for magnetostrictive phase and (101) for BTO were also calculated using Debye–Scherrer formula. All these results have been shown in Table 1.

HRTEM micrographs for sample A have been shown in Fig. 2. While Fig. 2.a depicts a bunch of core-shell type of particles, a single core-shell particle can be seen in Fig. 2.b.

The average diameter of the core corresponding to CFO is ~30 nm and the thickness of a more or less uniform shell of BTO has been found to be less than 10 nm here. Clear interface between the two phases and lattice planes in CFO are prominent in Fig. 2.c. Fig. 2.c shows an enlarged view of the interface in Fig. 2.b which clearly reveals the planes of both phases ([220], and [101] planes corresponding to CFO and BTO respectively). These planes have been identified and indexed based on the calculation of inter-planar spacing using ImageJ software. Insets in Fig. 2.c. present the Fast Fourier Transform (FFT) images of these planes of CFO and BTO.

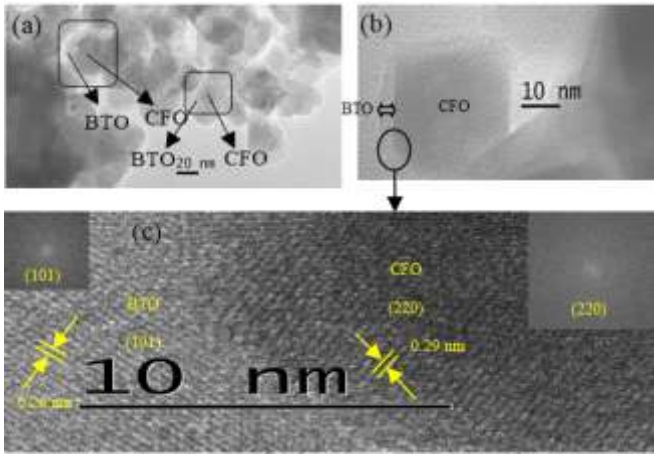

Fig. 2. (a), (b), and (c) HRTEM micrographs corresponding to sample A

EDX spectra in Fig. 3.a, 3.b and 3.c show the presence of all constituent elements in CFO, CFMO and BTO respectively without any trace of impurities. Same spectra for sample A and sample B have been shown in Fig. 3.d and 3.e respectively where peaks of all individual constituent elements of both phases are indexed. Here we can mention that the EDX spectrum for sample A was taken while HRTEM micrograph for the same was being recorded at the interface (Fig. 2.b). The weight percentage and the atomic percentage of all elements in these samples from EDX analysis have been tabulated in Table 2. They are in good agreement with our proposed composition of the samples. SEM micrographs of all the samples in powder form before sintering have been shown in Fig. 4. Agglomeration in CFO

Table 1 Average crystallite sizes, lattice parameters, saturation magnetization and coercivity of the samples

Sample	Average Crystallite sizes (nm)		Lattice parameters (Å)			M_S	M_R	H_C
	$CoFe_2O_4$	$BaTiO_3$	$CoFe_2O_4$	$BaTiO_3$		(emu/g)	(emu/g)	(Oe)
			a	a	c			
CFO	16		8.370			29.9	6.3	342.1
CFMO	14		8.351			22.2	3.6	211.3
A	17	17	8.352	4.0147	4.015	6.3	2.2	654.1
B	29	21	8.384	4.0126	4.0169	5.3	1.5	606.9
C	29	24	8.385	4.0288	4.022	10.1	3.8	711.9
D	15	17	8.370	4.026	4.0213	6.4	2.7	805
BTO		17		3.9679	4.0352			

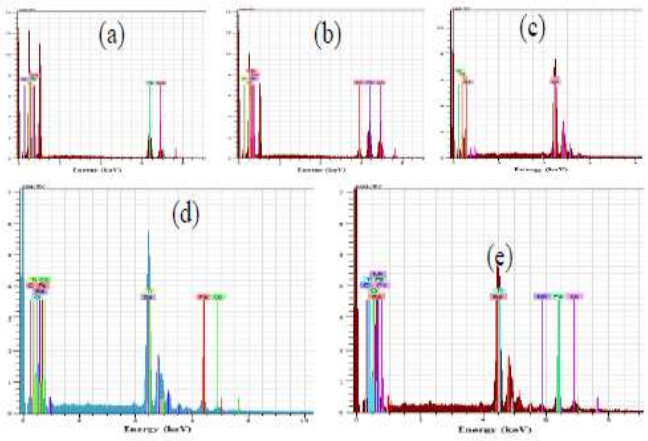

Fig. 3. EDX spectra of (a) CFO, (b) CFMO, (c) BTO, (d) sample A and (e) sample B

is quite clear (Fig. 4.b) which is due to the presence of nanomagnets in CFO nanoparticles [8]. Presence of both phases is evident in Fig. (d), (e), (f) and (g) where grains with brighter contrast correspond to BTO grains and grains with less brightness are of CFO and CFMO. Fig. 5 combines SEM micrographs of pellet form of all these samples after sintering above 1100°C. While some melting in individual core materials (Fig. 5.a and 5.b) can be seen besides particle formation, particles of spherical shape are visible in BTO (Fig. 5.c). In all composites, particles of two phases and dense microstructure are prominent features.

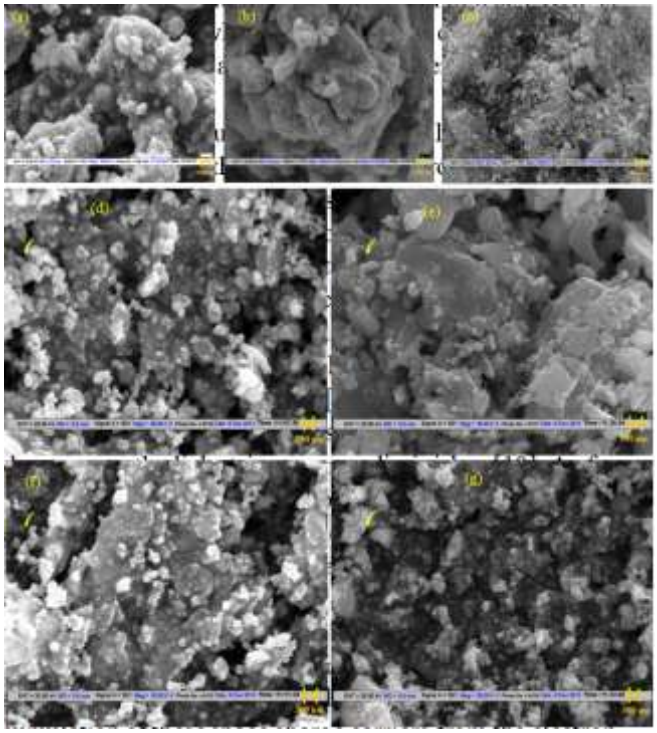

Fig. 4. Scanning Electron Micrographs for (a) BTO, (b) CFO, (c) CFMO, (d) sample A, (e) sample C, (f) sample B and (g) sample D in powder form

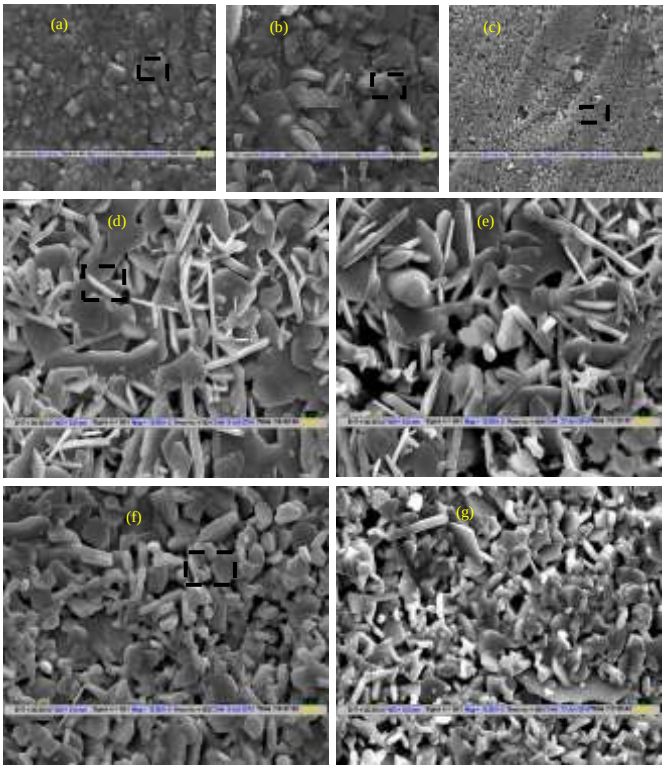

Fig. 5. Scanning Electron Micrographs for (a) CFO, (b) CFMO, (c) BTO, (d) sample A, (e) sample C, (f) sample B and (g) sample D in pellet form

Fig. 6 shows the variation of dielectric constant (ε) and tangent of dielectric loss angle (tanδ) with temperature (T) of all the composites at different frequencies. The variation is plotted in the temperature range 25°C - 500°C for ten fixed frequencies (i.e. 1 kHz, 3 kHz, 5 kHz, 10 kHz, 30 kHz, 50 kHz, 100 kHz, 300 kHz, 500 kHz and 1 MHz). For all samples, ε increases with increase in temperature and decrease in frequency. But around 485°C, the variation of ε shows some anomaly for sample B (Fig. 6.b) and sample D (Fig. 6.d). A prominent dip in the variation of ε at 1 KHz is found in Fig. 6.d which continuously diminishes with increase in frequency as can be clearly seen in the inset of Fig. 6.d.

The constancy in ε value below 200°C for all samples can be attributed to the fact that the overall microstructure of the composites remains more or less same in this temperature regime. Above 200°C, the role of ferrite phase comes into play in increasing dielectric constant value of the composites as the thermal energy starts to catch up with the potential barrier related to domain wall movement. It reaches a maximum around 480°C which is the magnetic Curie temperature (T_C) for CFMO [9]. Above T_C, magnetic domains disappear as the ferrites attain paramagnetic state and consequently dielectric response diminishes [10]. As far as the frequency response is concerned (Fig. 7.a), larger dielectric response at lower frequencies for all composites is due to well-known Maxwell-Wagner relaxation of charge accumulation at the interface [8]. The hopping electrons in ferrite come from the electron exchange $Fe^{2+} \Leftrightarrow Fe^{3+} + e^{-1}$ which are responsible for polarization through their displacements under applied electric field. Now, accumulation of these space charge carriers from the electron exchange along the direction of the applied field is time dependent. If the frequency of the alternating electric field becomes so high that these space charge carriers do not get enough time to align themselves along the direction of polarization and virtually become motionless, value of polarization decreases automatically [11]. Basically this is also the reason why the change in dielectric response around T_C is more prominent in lower frequencies as shown in Fig. 6.d. A particularly interesting feature of this anomaly here is that ε drastically moves to negative region around magnetic T_C momentarily and starts to return to positive value in a brief span of 10°C. Thus it shows trait of a meta-material in the vicinity. Again a prominent hump is found around 230°C in dielectric loss response for sample C which contains the maximum weight percentage of CFO among the composites (Fig. 6.g). This is due to hopping of electrons in between A and B sub lattices of ferrite [6]. This feature is present but less visible in other composites (Fig. 6.c, 6.d and 6.h). Relaxation peaks in frequency response of dielectric loss of the samples in Fig. 7.b also occur due to this electron hopping phenomenon in ferrite [11].

Table 2. Quantitative elemental analysis using EDX spectra for CFO, CFMO, BTO, CFO-BTO_30%, and CFMO-BTO_30%

Fig.	Element	Weight%	Atomic%
3.a	O K	64.45	77.57
	Co K	9.87	3.23
	Fe K	17.45	6.02
3.b	O K	49.04	67.96
	Co K	17.82	6.70
	Fe K	20.30	8.06
	Mn K	4.46	1.80
3.c	O K	26.67	50.72
	Ba L	48.32	10.71
	Ti K	13.06	8.30
3.d	O K	34.23	57.04
	Ba L	40.38	7.84
	Ti K	13.53	6.93
	Co K	1.20	0.65
	Fe K	3.18	1.43
3.e	O K	27.07	51.55
	Ba L	44.84	9.95
	Ti K	14.46	9.12
	Co K	2.90	1.50
	Fe K	4.81	2.62
	Mn K	1.04	0.58

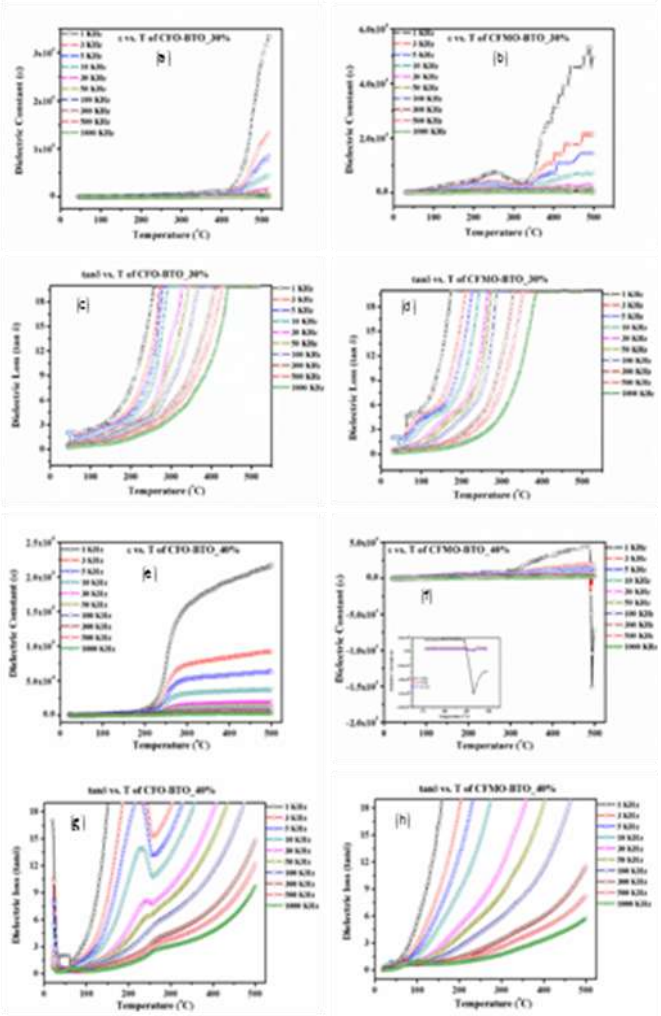

Fig. 6. Variation of dielectric constant (ε) with temperature (T) for (a) sample A, (b) sample B, (e) sample C, (f) sample D and of tangent of dielectric loss angle (tanδ) with temperature (T) for (c) sample A, (d) sample B, (g) sample C, (h) sample D at different frequencies

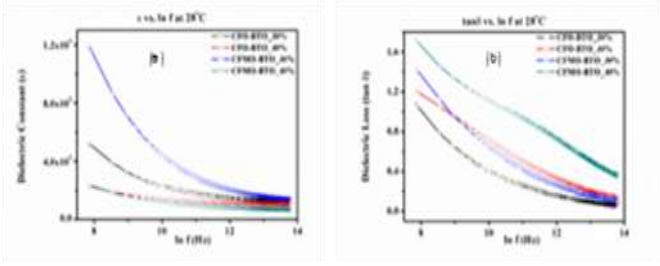

Fig. 7. Variation of dielectric constant (ε) with frequency for (a) sample A, sample B, sample C and sample D and of tangent of dielectric loss angle (tanδ) with frequency for (b) sample A, sample B, sample C and sample D at room temperature

Magnetic hysteresis loops of individual ferrites and composites have been shown in Fig. 8. Measurements were done at room temperature and a magnetic field was scanned in the range -5000 Oe to +5000 Oe. As expected, all the loops are ferromagnetic in nature with higher magnetization and lower coercivity for the ferrites than their corresponding composites. The magnetization values (M_S) at 5000 Oe and coercive fields (H_C) for all the samples are tabulated in Table 1. Clearly, presence of BTO in the composites accounts for the loss of their ferromagnetic behavior. Though the highest magnetizations achieved here for all samples have not reached saturation, it is still very clear that they are way below than their bulk saturation magnetization values (i.e. M_S for bulk CFO ~ 65 emu/g). The reason might be the formation of magnetic nanoparticles with very small crystallite sizes relative to their bulk counterparts which gives rise to various factors, such as dead layer formation because of very high surface to volume ratio, canting of electron spin at the surface etc. [11,12] that bring down the saturation magnetization value. These factors are collectively and commonly known as size or surface effects [13].

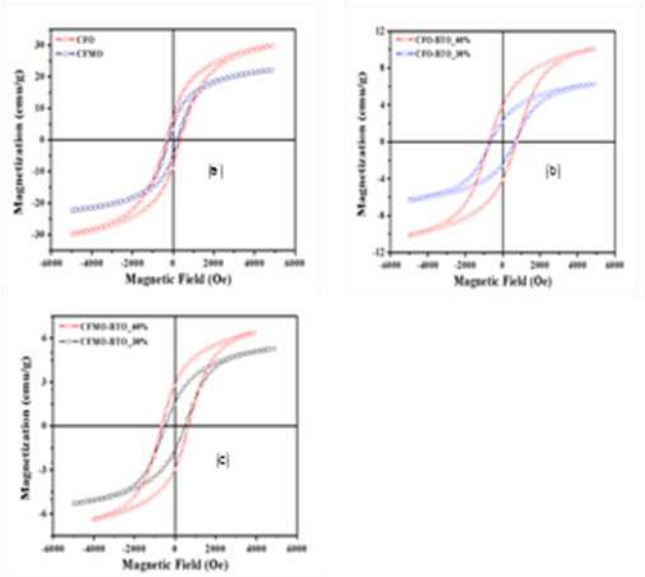

Fig. 8. Magnetization (M) vs. magnetic field (H) plot for (a) CFO and CFMO, (b) sample A and C, (c) sample B and D

All these samples were subjected to an excitation wavelength of 266 nm and corresponding recorded PL spectra have been presented in Fig. 9. Since the energy band gap (E_g) of bulk BTO is typically in the range 2.9–3.4 eV, the luminescence states lie well within E_g. So with an excitation wavelength of 266 nm, the PL spectrum of BTO consists of a prominent emission peak, centered at 373 nm which is accompanied by a shoulder at the receding edge. It can be attributed to the presence of O-Ti-O network which is intermediately formed during the formation of oxygen octahedra (TiO_6), enclosing Ti^{4+} ion [14]. Emission peak corresponding to pure CFO is centered at 370 nm and results from the presence of quantum confinement that has energy of the order of band gap of ferrite materials (~3 eV)[15,16]. Mn substitution broadens this peak (Fig. 9.b) as Mn^{3+} ions work as electron traps and give rise to intermediate energy levels [17]. In case of composites, the emission profiles are clearly identical to that of BTO, reflecting the core-shell nature of the samples with BTO encapsulating the ferrites. The excitation wavelength of 266 nm was, most probably, unable to penetrate the shell of BTO which has an average thickness of 10 nm as we have seen in the HRTEM micrograph (Fig. 2.b). But as the amount of ferrites increases in the composites, we can notice that the prominent shoulder in pure BTO starts to diminish. Another peak appears around 470 nm (~ 2.66 eV) for all the samples which can be attributed to the presence of singly charged oxygen vacancies. Doubly ionized oxygen vacancies are most common form of defects in perovskites and spinels [18]. They tend to neutralize when treated in high temperature post synthesis. It may so happen during this process that some of the doubly ionized vacancies undergo incomplete neutralization and become singly charged. They are responsible for this peak around 470 nm [19]. These spectra have been reported for the first time for these composites.

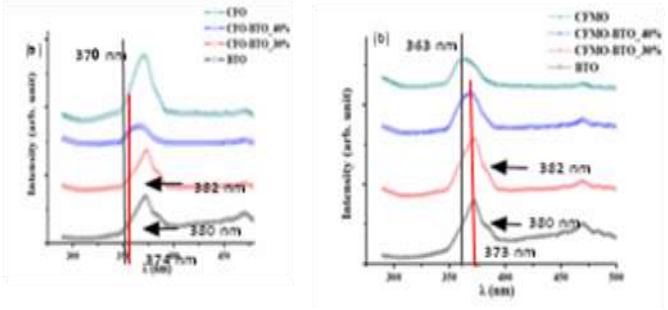

Fig. 9. Photoluminescence spectra for (a) CFO, BTO, sample A, sample C and (b) CFMO, BTO, sample B, sample D using a laser excitation source of 266 nm

IV. CONCLUSION

To summarize, CFO-BTO and CFMO-BTO composites were synthesized by conventional wet chemical method. XRD analysis shows presence of prominent spinel peaks corresponding to CFO and CFMO and perovskite peaks for BTO. Average crystallite sizes and lattice parameters of the phases were calculated and found to be in good agreement with previous work by other researchers. HRTEM micrographs show existence of proposed core-shell nature of sample. All peaks corresponding to constituent elements of both phases are present in EDX spectra. SEM micrographs of powders as well as pellets indicate presence of two different phases in the composites. A prominent dip has been found in the response of ε with temperature around magnetic T_C for CFMO-BTO composite and negative ε has been achieved momentarily. M-H plots reveal ferromagnetic nature of all the samples with much lower saturation magnetization value than their bulk counterparts. Finally, PL spectra were recorded for these composites for the first time. The nature of the plots is clearly indicative of the core-shell nature of the composites.

ACKNOWLEDGEMENTS

Authors would like to acknowledge Nano Science Unit of NSTI, DST, IIT Delhi for acquiring HRTEM micrographs. They would like to thank Prof. Ratnamala Chatterjee in IIT Delhi for the dielectric measurements. Optical characterization was carried out under Nanophotonic material high-impact research scheme of IIT Delhi. One of the authors (SS) acknowledges CSIR, India for providing fellowship.

REFERENCES

1. J.Ma, J. Hu, Z. Li, C. W. Nan, Recent progress in multiferroic magnetoelectric composites: From bulk to thin films, Adv. Mater. 23 (2011) 1062-1087.
2. J.Ryu, S.Priya, K. Uchino, H.E. Kim, Magnetoelectric effect in composites of magnetostrictive and piezoelectric materials, J. Electroceram. 8 (2002) 107-119.
3. W. Eerenstein, N. D. Mathur, J. F. Scott, Multiferroic and magnetoelectric materials, Nature 442 (2006) 759-765.
4. N. A. Spaldin, M.Fiebig, The renaissance of magnetoelectric multiferroics, Science 309 (2005) 391-392.

5. Gupta, R. Chatterjee, Study of dielectric and magnetic properties of $PbZr_{0.52}Ti_{0.48}O_3$–$Mn_{0.3}Co_{0.6}Zn_{0.4}Fe_{1.7}O_4$ composite, J. Magn. Magn. Mater. 322 (2010) 1020–1025.
6. Gupta, R. Chatterjee, Dielectric and magnetoelectric properties of BaTiO3–Co0.6Zn0.4Fe1.7Mn0.3O4 composite, J. Eur. Ceram. Soc. 33 (2013) 1017-1022.
7. V. C. Flores, D. B. Baque´s, R. F. Ziolo, Synthesis and characterization of novel $CoFe_2O_4$–$BaTiO_3$ multiferroic core–shell-type nanostructures, Acta. Mater. 58 (2010) 764–769.
8. V. V. Shvartsman, F. Alawneh, P. Borisov, D. Kozodaev, D. C. Lupascu, Converse magnetoelectric effect in $CoFe_2O_4$–$BaTiO_3$ composites with a core–shell structure, Smart. Mater. Struct. 20 (2011) 075006.
9. O. Caltun, G.S.N. Rao, K.H. Rao, B.P. Rao, I. Dumitru, C.G. Kim, Manganese substituted cobalt ferrite for sensor applications, J. Magn. Magn. Mater. 320 (2008) 869.
10. R. S. Devan, S. B. Deshpande, B.K.Chougule, Ferroelectric and ferromagnetic properties of (x) $BaTiO_3$ + (1 − x) $Ni_{0.94}Co_{0.01}Cu_{0.05}Fe_2O_4$ Composite, J. Phys. D. Appl. Phys. 97 (2010) 062904.
11. H. Gul, A. Maqsood, Structural, magnetic and electrical properties of cobalt ferrites prepared by the sol–gel route, J. Alloy. Compd. 465 (2008) 227–231.
12. R. Gupta, J. Shah, S. Chaudhary, S. Singh, R. K. Kotnala, Magnetoelectric coupling-induced anisotropy in multiferroic nanocomposite (1 - x)BiFeO3–xBaTiO3, J. Nanopart. Res. 15:2004 (2013).
13. M. K. Surendra, D. Kannan, M. S. R. Rao, Magnetic and dielectric properties study of cobalt ferrite nanoparticles synthesized by co-precipitation method, Mater. Res. Soc. Symp. P. 1368 (2011).
14. S. I. Seok, M. S. Kim, T. S. Suh, Photoluminescence probing of the formation of titanium dioxide sols from a titanium peroxide solution, J. Am. Ceram. Soc. 85 (2002) 1888-1890.
15. R. K. Singh, A. Narayan, K. Prasad, R. S. Yadav, A. C. Pandey, A. K.Singh, L. Verma, R. K. Verma, Thermal, structural, magnetic and photoluminescence studies on cobalt ferrite nanoparticles obtained by citrate precursor method, J. Therm. Anal. Calorim. 110 (2012) 573-580.
16. Y. Fu, H. Chen, X. Sun, X. Wang, Combination of cobalt ferrite and graphene: High-performance and recyclable visible-light photocatalysis, Appl. Catal. B-Environ. 111–112 (2012) 280– 287.
17. N. V. Dang, The-Long Phan, T. D. Thanh, V. D. Lam, L. V. Hong, Structural phase separation and optical and magnetic properties of $BaTi_{1-x}Mn_xO_3$ multiferroics, J. Appl. Phys. 111 (2012) 113913.
18. W. L. Warren, K. Vanheusden, D. Dimos, G. E. Pike, B. A. Tuttle, Oxygen vacancy motion in perovskite oxides, J. Am. Ceram. Soc. 79 (1996) 536-538.
19. Vanheusden, W. L. Warren, C. H. Seager, D. R. Tallant, J. A. Voigt, B. E. Gnade, Mechanisms behind green photoluminescence in ZnO phosphor powders, J. Appl. Phys. 79 (1996) 7983.

AUTHOR PROFILE

Sourav Sarkar received his Bachelor of Science (Hons) degree in Physics from Calcutta University, India and Master of Science (M.Sc) degree in Physics from Indian Institute of Technology, Delhi (IIT Delhi), India in 2008 and 2010 respectively. He was joint recipient of Jagat Ram Chopra Award for Best Thesis by a Master's student at IIT Delhi in 2010. He is currently pursuing his Ph.D from Physics Department, IIT Delhi. His broad area of research includes Multiferroic Composite materials, and Ferrite based Sensors.

Dr. Jyoti Shah is currently working as DST-Women Scientist at CSIR-National Physical Laboratory, India. She has authored more than 75 journal papers. An expert in numerous characterization techniques, her research interest includes Material Science, Spectroscopy, Thin Films, Nanotechnology and Nanomaterials, and many more.

Dr. R. K. Kotnala is a Chief Scientist (Scientist for last 33 years in NPL, New Delhi) & Head of Materials Physics & Engineering Division, National Physical Laboratory, New Delhi. He obtained Ph.D in Solar Cell from IIT Delhi in 1982. He is an Associate Editor for last two years in Journal of Applied Physics, AIP, NewYork, USA. He has published 305 research papers in prestigious international journals, has 681 citations only in last 10 months, has 6 US/ Indian patents, 9 industrial consultancies & support to 112 industries. He has given more than 310 invited talks, and has authored 4 books. His areas of specialization are Magnetic Measurements standards, Nano Magnetic Material, Superconductivity, Multiferroics, CMR Materials, DMS, Spintronic Device Physics, Solar Cell, Humidity Sensor, and Hydroelectric Cell.

Dr. M.C. Bhatnagar is an Associate Professor at the department of Physics, IIT Delhi. He received his M.Sc (Physics) and M.Tech (Microwave Engineering) from University of Delhi and PhD in the field of solar cells from IIT Delhi. His current area of research includes development of humidity and gas sensors, ferrite based sensors, associated electronics and instrumentation, and gas sensitivity improvement by ion beam irradiation.

Published By:
Blue Eyes Intelligence Engineering
& Sciences Publication